Applied Mathematics and Computation 437 (2023) 127523

Contents lists available at ScienceDirect

Applied Mathematics and Computation

journal homepage: www.elsevier.com/locate/amc

A simulation expressivity of the quenching phenomenon in a two-sided space-fractional diffusion equation

Lin Zhu[a,*], Nabing Liu[a], Qin Sheng[b]

[a] School of Mathematics and Statistics, Ningxia University, Yinchuan 750021, China
[b] Department of Mathematics and Center for Astrophysics, Space Physics and Engineering Research, Baylor University, Waco, TX 76798-7328, USA

ARTICLE INFO

Article history:
Received 20 January 2022
Revised 13 July 2022
Accepted 1 September 2022

Keywords:
Nonlinear quenching problems
Two-sided Riemann-Liouville space-fractional derivatives
Mesh adaptation
Stability
Positivity
Monotonicity

ABSTRACT

The aims of this paper are to investigate and propose a numerical approximation for a quenching type diffusion problem associated with a two-sided Riemann-Liouville space-fractional derivative. The approach adopts weighted Grünwald formulas for suitable spatial discretization. An implicit Crank-Nicolson scheme combined with adaptive technology is then implemented for a temporal integration. Monotonicity, positivity preservation and linearized stability are proved under suitable constraints on spatial and temporal discretization parameters. Two specially designed simulation experiments are presented for illustrating and outreaching properties of the numerical method constructed. Connections between the two-sided fractional differential operator and critical values including quenching time, critical length and quenching location are investigated.

1. Introduction

Quenching phenomena can be observed in many scientific and industrial disciplines, such as cell multiplications, liquid and solid fuel combustion, pipeline decay preventions and infectious disease outbreak controls. The phenomena have attracted a tremendous amount of recent attentions due to their profound applications to nature and engineering technologies [1–5].

In his pioneering study of quenching modelings, Kawarada noticed that for the reaction-diffusion equation $u_t = u_{xx} + 1/(1-u),\ 0 < x < a,\ t > 0$, there exists a critical domain size $a^\star > 2\sqrt{2}$ such that for any $a > a^\star$, we have $\sup\{\lim_{t\to T_a^-} u\} = 1,\ T_a < \infty$ [4,6], no matter how small the initial and boundary values are. Acker and Walter later reconfirmed this observation and found that $a^\star$ was approximately 1.5303 via numerical simulations [1].

It is crucial in quenching simulations to predict correlated key ingredients, such as critical domain size, location and quenching time of an anticipated quenching, and the impact of potential stochastic interferences in approximations of a quenching solution [7–9]. In addition, numerical methods must capture characteristical features of the quenching phenomena, such as the quenching domain sizes, and preservations of the solution monotonicity, positivity in certain situations (for instance, see [2,10–12] and references therein).

Finite difference and boundary element methods have been used in the classical quenching numerical methods [8,10]. Results obtained have significantly extended the original work by Hale [4], Kawarada [6], Chan and Chen [10], Walter [12].

* Corresponding author.
E-mail addresses: zhul@nxu.edu.cn (L. Zhu), liunb@stu.nxu.edu.cn (N. Liu), qin_sheng@baylor.edu (Q. Sheng).

https://doi.org/10.1016/j.amc.2022.127523
0096-3003/

Needless to mention that many existing algorithms become successively complicated when higher dimensional problems are considered. To this end, mesh adaptations are introduced to improve the computational efficiency and accuracy [13]. Simulation strategies are also benefitted from the theory and methods of domain decompositions and exponential splitting formulations [2,14,15]. Semi-discretization and linear iterations are employed to reduce the complexity of the implicit schemes acquired [16,17]. However, bottleneck difficulties continue existing, such as that in linear and nonlinear numerical instabilities while simpler-structured and easier-to-use algorithms are in demands for realistic industrial and environmental applications [8,18,19].

Many integer order partial differential equation models can be extended to fractional order partial differential equations (FPDEs) for possibly more natural approximations of real phenomena. FPDEs have been particularly widely utililzed in image processing, thermal engineering products, electrochemistry, generic memory designs, and medicine devices [20,21]. In particular, Meerschaert and Tadjeran introduced and analyzed two-side space-fractional partial differential equations and approximations [22]. Following their work, Zhu and Rui introduced the weighted Grünwald approximation for the two-sided space-fractional derivatives [23]. An effective maximum modulus principle is established for finite difference methods to solve fractional equations [24]. Based on it, the existence and regularities of the solutions are guaranteed [23]. However, in the territory of singular FPDEs, especially those involving strong nonlinear quenching singularities, studies in regularities are still in its infancy while simulation approaches are booming [20,22,25,26]. Among the most recent publications, Padgett approximated singular solutions to a Kawarada equation with fractional derivative of the Caputo type in time [7]. Xu focused at fractional diffusion operators and their quenching applications [9]. The many heuristic discussions on fractional ordered differential equations have quickly become an intensive research field attracting more and more attentions for in-depth theory and simulations [21,26].

In this paper, we are concerned with FPDEs where nonlocal α-fractional two-sided derivative, $1 < \alpha \le 2$, is used to replace the conventional Laplacian operator in a Kawarada equation. Backgrounds of such fractional modeling structure can be found in several recent publications including [20,22,23,27,28].

Both theoretical and numerical explorations will be carried out for the stability, positivity and monotonicity of the semi-adaptive scheme proposed. The simulation strategies are more balanced and effective as compared to typical configurations used in traditional one-sided approaches by Zhu and Sheng [28], and adaptations by Huang et al. [13], Beauregard [29]. Simulation results will be provided to illustrate adjustments between situations with conventional and fractional derivatives. Anticipated critical values including fractional quenching location, time and critical length will be given and discussed. The solution symmetry, which is an important geometric feature of the quenching solution [4,11,30], is preserved in all numerical experiments. Our results acquired agree satisfactorily with known results of compatible integer order problems [8,11].

The present discussion consists of six sections. A two-sided fractional order quenching model will be introduced in Section 2. In Section 3, a semi-adaptive finite difference approximation will be constructed. Numerical stability of the simulation method will be analyzed. Section 4 will focus on the quenching characteristics including the solution positivity, monotonicity, and quenching domains and times. Detailed analysis will be presented. In Section 5, typical modeling fractional problems associated with a two-sided Riemann-Liouville space-fractional derivative will be simulated. Numerical solutions and correlated critical values will be obtained and explained. Brief concluding remarks and expectations of continuing work will be summarized in Section 6.

2. Semi-adaptive numerical method

Consider the following two-sided space-fractional order diffusion equation

$$\frac{\partial w(x,t)}{\partial t} = c_-(x,t)\frac{\partial^\alpha w(x,t)}{\partial_- x^\alpha} + c_+(x,t)\frac{\partial^\alpha w(x,t)}{\partial_+ x^\alpha} + s(w), \tag{2.1}$$

where $\alpha \in (1,2]$, $s(w) = 1/(1-w)$, $c_+(x,t) \ge 0$, $c_-(x,t) \ge 0$, $x \in (0,a)$, $0 < t \le T < \infty$, and $\frac{\partial^\alpha w(x,t)}{\partial_- x^\alpha}$, $\frac{\partial^\alpha w(x,t)}{\partial_+ x^\alpha}$ are right- and left-handed Riemann-Liouville fractional derivatives, respectively [22,27]. It is known that solutions of the semi-linear Eq. (2.1) exist and are unique if s satisfies the Lipschitz condition prior to quenching and well-posted initial-boundary conditions are used [20,23,31]. We also note that when $1 < \alpha < 2$, (2.1) represents a super-diffusive case which implies that particles diffuse faster than the classical case when $\alpha = 2$ [32].

The differential equation can be viewed as an extension of the original and one-sided Kawarada equations [6,28]. It is also a realization of the diamond derivative formula [33]. Similar to [4,11], we adopt following homogeneous first boundary conditions

$$w(0,t) = w(a,t) = 0, \qquad 0 < t \le T < \infty. \tag{2.2}$$

A straightforward initial condition,

$$w(x,0) = \phi(x), \qquad x \in [0,a], \tag{2.3}$$

where $0 \le \phi(x) \ll 1$ is considered.

Let $K, M \in \mathbb{Z}^+$ and set $h = a/K$, $\tau = T/M$. We define that

$$x_i = ih,\ i = 0,1,\ldots,K;\ t_k = k\tau,\ k = 0,1,\ldots,M.$$

While denoting $a_i = c_-(x_i,t)$, $b_i = c_+(x_i,t)$ and $s_i = s(w_i)$, we let w_i be a numerical approximation of $w(x_i,t)$, $i = 0,1,\ldots,K$.

We approximate the two-sided fractional order derivatives by weighted averaging approximations via shifted Grünwald formulas with second-order accuracy [24,25]. In particularly,

$$\begin{aligned}\frac{\partial^\alpha w(x_p,t)}{\partial_+ x^\alpha} &= \frac{1}{h^\alpha}\left[\left(1-\frac{\alpha}{2}\right)\sum_{i=0}^{p} g_i w_{p-i} + \frac{\alpha}{2}\sum_{i=0}^{p+1} g_i w_{p-i+1}\right] + \mathcal{O}(h^2);\\ \frac{\partial^\alpha w(x_p,t)}{\partial_- x^\alpha} &= \frac{1}{h^\alpha}\left[\left(1-\frac{\alpha}{2}\right)\sum_{i=0}^{K-p} g_i w_{p+i} + \frac{\alpha}{2}\sum_{i=0}^{K-p+1} g_i w_{i+p-1}\right] + \mathcal{O}(h^2),\end{aligned} \tag{2.4}$$

where $h \to 0^+$ and

$$g_i = \frac{\Gamma(i-\alpha)}{\Gamma(-\alpha)\Gamma(i+1)} = (-1)^i\binom{\alpha}{i} = (-1)^i\frac{(\alpha)(\alpha-1)\ldots(\alpha-i+1)}{i!},$$
$$i = 0,1,\ldots,K,$$

and the set $\{g_i\}$ satisfies following properties:

$$\begin{cases} g_0 = 1,\\ g_1 = -\alpha < 0,\\ 1 \geq g_2 \geq g_3 \geq \ldots \geq 0,\\ \sum_{i=0}^{M} g_i \leq 0,\ M \in \mathbb{Z}^+,\\ \sum_{i=0}^{\infty} g_i = 0. \end{cases} \tag{2.5}$$

A substitution of (2.4) into (2.1) yields

$$\begin{aligned}(w_t)_p = {}& \frac{a_p}{h^\alpha}\left[\left(1-\frac{\alpha}{2}\right)\sum_{i=0}^{p} g_i w_{p-i} + \frac{\alpha}{2}\sum_{i=0}^{p+1} g_i w_{p-i+1}\right]\\ &+\frac{b_p}{h^\alpha}\left[\left(1-\frac{\alpha}{2}\right)\sum_{i=0}^{K-p} g_i w_{i+p} + \frac{\alpha}{2}\sum_{i=0}^{K-p+1} g_i w_{i+p-1}\right] + s_p + \mathcal{O}(h^2),\end{aligned} \tag{2.6}$$

for $p = 1,2,\ldots,K$. Drop the truncation error. Together with (2.2) and (2.3), the above can be reformulated to yield the following initial value problem

$$w_t = Hw + s(w),\ 0 < t < T,\ w(0) = w_0, \tag{2.7}$$

where $w = (w_1, w_2, \ldots, w_K)^\intercal$, $s = (s_1, s_2, \ldots, s_K)^\intercal \in \mathbb{R}^K$ and $H = (h_{ij}) \in \mathbb{R}^{K\times K}$. For the coefficient matrix we have

$$h_{ij} = \begin{cases} \frac{a_i+b_i}{h^\alpha}\left[\left(1-\frac{\alpha}{2}\right)g_0 + \frac{\alpha}{2}g_1\right], & i = j,\\ \frac{b_i\alpha}{2h^\alpha}g_0 + \frac{a_i}{h^\alpha}\left[\left(1-\frac{\alpha}{2}\right)g_1 + \frac{\alpha}{2}g_2\right], & i = j+1,\\ \frac{a_i\alpha}{2h^\alpha}g_0 + \frac{b_i}{h^\alpha}\left[\left(1-\frac{\alpha}{2}\right)g_1 + \frac{\alpha}{2}g_2\right], & i = j-1,\\ \frac{b_i}{h^\alpha}\left[\left(1-\frac{\alpha}{2}\right)g_{j-i} + \frac{\alpha}{2}g_{j-i+1}\right], & i < j-1,\\ \frac{a_i}{h^\alpha}\left[\left(1-\frac{\alpha}{2}\right)g_{i-j} + \frac{\alpha}{2}g_{i-j+1}\right], & i > j+1. \end{cases} \tag{2.8}$$

The formal solution of (2.7) has the following form Iserles [34], LeVeque [35]

$$w(t) = e^{Ht}w_0 + \int_0^t e^{H(t-\phi)}s(w)d\phi, \quad t \geq 0. \tag{2.9}$$

The Eq. (2.9) can approximated through a trapezoidal rule, that is,

$$w(t) = e^{Ht}w_0 + \frac{t}{2}\left[s(w(t)) + e^{Ht}s(w_0)\right] + \mathcal{O}(t^2),\ t \geq 0.$$

Using an A [1/1] Padé approximant to evaluate the matrix exponential e^{Ht} as following,

$$e^{Ht} = \left(I - \frac{t}{2}H\right)^{-1}\left(I + \frac{t}{2}H\right) + \mathcal{O}(t^2), \quad t \to 0^+. \tag{2.10}$$

A second-order difference scheme is consequently determined as

$$w_k = \left(I - \frac{\tau_k}{2}H\right)^{-1}\left(I + \frac{\tau_k}{2}H\right)\left(w_{k-1} + \frac{\tau_k}{2}s_{k-1}\right) + \frac{\tau_k}{2}s_k,\ k = 1,2,\ldots,M, \tag{2.11}$$

for which $w_0 = (w_1(0), w_2(0), \ldots, w_K(0))^\intercal$, and $0 < \tau_k = t_k - t_{k-1} \ll 1,\ k \in \{1, 2, \ldots, M\}$. Owing to a Taylor expansion based linearization of the nonlinear source term, $s_k \approx s(w_{k-1} + \tau_k(Hw_{k-1} + s_{k-1}))$, the overall truncation error of (2.11) may be reduced to $\mathcal{O}(h^2 + \tau_k)$ [8,14]. Similar to those discussed in [2,3,30,36], we adopt a w_t-based arc-length monitor function for temporal adaptations:

$$p(w_t, t) = \max_{0\le x\le a} \sqrt{1 + w_{tt}^2}, \quad t \ge t_0.$$

The following quadratic formulation is desirable for calculating variable adaptive time increments τ_{k+1} :

$$\tau_{k+1}^2 = \frac{1 + \max_{0\le x\le a}\left(w_{tt}(t_{k-1/2})\right)^2}{1 + \max_{0\le x\le a}\left(w_{tt}(t_{k+1/2})\right)^2}\,\tau_k^2, \quad k = 0, 1, 2, \ldots, M-1. \tag{2.12}$$

If $\tau_0 > 0$ is identified, subsequent adaptive time increments can be evaluated via (2.12) recursively. Appropriate constraints for a smooth adaptation must be observed [8,13,29]. The time increments are expected to be small throughout the final stage of simulations since that $0 \ll \max_{0\le x\le a} w(x,t) < 1$.

3. Stability

Theorem 3.1. *If* $\frac{\sqrt{17}-1}{2} \le \alpha \le 2$ *then* $I - \frac{\tau_k}{2}H$ *is strictly diagonally dominant, inverse positive and monotone* [23], *24*, *28*.

Proof. Note that for $1 < \alpha \le 2$, we have

$$\frac{\alpha^2}{2} + \frac{\alpha}{2} - 1 > 0.$$

Denote $D = I - \frac{\tau_k}{2}H$. We consider diagonal and off-diagonal elements of D :

$$\begin{aligned}
d_{ii} &= 1 + \frac{\tau_k(a_i + b_i)}{2h^\alpha}\left(\frac{\alpha^2}{2} + \frac{\alpha}{2} - 1\right),\\
d_{i,i-1} &= -\frac{\tau_k b_i \alpha}{4h^\alpha} - \frac{\tau_k a_i \alpha}{2h^\alpha}\left(\frac{\alpha^2 + \alpha - 4}{4}\right),\\
d_{i,i+1} &= -\frac{\tau_k a_i \alpha}{4h^\alpha} - \frac{\tau_k b_i \alpha}{2h^\alpha}\left(\frac{\alpha^2 + \alpha - 4}{4}\right),\\
d_{i,p} &= -\frac{\tau_k b_i}{2h^\alpha}\left[\left(1 - \frac{\alpha}{2}\right)g_{p-i} + \frac{\alpha}{2}g_{p-i+1}\right], \quad \text{if } p > i+1;\\
d_{i,p} &= -\frac{\tau_k a_i}{2h^\alpha}\left[\left(1 - \frac{\alpha}{2}\right)g_{i-p} + \frac{\alpha}{2}g_{i-p+1}\right], \quad \text{if } p < i-1,\\
&\qquad \text{where } i, p \in \{1, 2, \ldots, K\} \text{ for all meaningful indexes.}
\end{aligned}$$

Similar to the case in [28], for $\frac{\sqrt{17}-1}{2} \le \alpha \le 2$ we have $\frac{\alpha^2}{2} + \frac{\alpha}{2} - 1 > 0$, $\frac{\alpha^2+\alpha-4}{4} \ge 0$ due to (2.5). Therefore $d_{i,i} > 0$, $d_{i,i+1} < 0$, $d_{i,i-1} < 0$.

By the same token, we observe that

$$\begin{aligned}
&\frac{\alpha}{2}g_{i-p+1} + \left(1 - \frac{\alpha}{2}\right)g_{i-p} > 0, \quad \text{if } p < i-1,\\
&\frac{\alpha}{2}g_{p-i+1} + \left(1 - \frac{\alpha}{2}\right)g_{p-i} > 0, \quad \text{if } p > i+1.
\end{aligned}$$

Hence, $d_{i,p} < 0$ for all $p > i+1$ or $p < i-1$ within the range of indexes.

Furthermore, we compute the absolute sums of off-diagonal elements of the matrix D :

$$\begin{aligned}
r_i &= \sum_{j=1, j\ne i}^{K} \left|d_{ij}\right| = \frac{\tau_k a_i}{2h^\alpha}\left\{\sum_{p=1}^{i-1}\left[\frac{\alpha}{2}g_{i-p+1} + \left(1 - \frac{\alpha}{2}\right)g_{i-p}\right] + \frac{\alpha}{2}g_0\right\}\\
&\quad + \frac{\tau_k b_i}{2h^\alpha}\left\{\sum_{p=i+1}^{K}\left[\frac{\alpha}{2}g_{p-i+1} + \left(1 - \frac{\alpha}{2}\right)g_{p-i}\right] + \frac{\alpha}{2}g_0\right\}\\
&\le \frac{\tau_k(a_i + b_i)}{2h^\alpha}\left(\frac{\alpha^2}{2} + \frac{\alpha}{2} - 1\right), \quad i = 1, 2, \ldots, K.
\end{aligned}$$

Thus,

$$r_i = \sum_{j=1, j\ne i}^{K} \left|d_{ij}\right| < \frac{\tau_k(a_i + b_i)}{2h^\alpha}\left(\frac{\alpha^2}{2} + \frac{\alpha}{2} - 1\right) + 1 = d_{ii}, \quad i = 1, 2, \ldots, K.$$

The above indicate that D is strictly diagonally dominant and invertible.

In above analysis, we may notice that elements of the matrix D possess desirable properties, such as all its diagonal elements are positive and the rest must be negative. In addition,

$$\begin{aligned}\sum_{j=1}^{K} d_{rj} &= 1-\frac{\tau_k a_r}{2h^\alpha}\left[\frac{\alpha}{2}(g_0+g_1+\cdots+g_r)+\left(1-\frac{\alpha}{2}\right)(g_0+g_1+\cdots+g_{r-1})\right]\\ &\quad-\frac{\tau_k b_r}{2h^\alpha}\left[\frac{\alpha}{2}(g_0+g_1+\cdots+g_r)+\left(1-\frac{\alpha}{2}\right)(g_0+g_1+\cdots+g_{r-1})\right]\\ &= 1-\frac{\tau_k(a_r+b_r)}{2h^\alpha}\left[\left(1-\frac{\alpha}{2}\right)\sum_{p=0}^{r-1} g_p+\frac{\alpha}{2}\sum_{p=0}^{r} g_p\right],\end{aligned}$$

where $r=1,2,\ldots,K-1$. Through (2.5). $\sum_{j=1}^{K} d_{rj}>0,\ r=1,2,\ldots,K-1$. In the particular case when $r=K$, this result can still be drawn by $\sum_{i=1}^{r} g_i \le -1$. This implies that D is monotone and inversely positive since matrix D satisfies the weak-row sum criterion [35]. Thus our proof is completed. □

Theorem 3.2. *Let* $\frac{\sqrt{17}-1}{2} \le \alpha \le 2$ *and* $\eta_{\alpha,k}=\max_k \frac{\tau_k}{h^\alpha}$. *If*

$$\eta_{\alpha,k} < \frac{1}{2\max\limits_{1\le i\le K}(a_i+b_i)} = \frac{1}{2(a_{\max}+b_{\max})} \tag{3.1}$$

then $I+\frac{\tau_k}{2}H$ *is nonsingular and positive.*

Proof. Set $E=I+\frac{\tau_k}{2}H=(e_{ij})_{K\times K}$. According to the proof of Theorem 3.1, it can be seen that all $h_{ij}>0, i\ne j,\quad i,j=1,2,\ldots,K$ due to (2.5) and (3.1). Subsequently $e_{ij}>0$ whenever $i\ne j,\quad i,j=1,2,\ldots,K$. Therefore we only need to analyze diagonal elements of the matrix E. To this end,

$$\begin{aligned}e_{ii} &= 1+\frac{\tau_k(a_i+b_i)}{2h^\alpha}\left[\left(1-\frac{\alpha}{2}\right)g_0+\frac{\alpha}{2}g_1\right] = 1-\frac{\tau_k(a_i+b_i)}{2h^\alpha}\left(\frac{\alpha^2}{2}+\frac{\alpha}{2}-1\right)\\ &\ge 1-\frac{\tau_k(a_i+b_i)}{h^\alpha},\quad i=1,2,\ldots,K.\end{aligned}$$

Thus, we have $e_{ii}>0$ based on (3.1). Therefore E is positive. Furthermore, the infinity-norm of $\frac{\tau_k}{2}H$ can be estimated as follows:

$$\begin{aligned}\left\|\frac{\tau_k}{2}H\right\|_\infty &= \frac{\tau_k}{2}\max_i\left\{\sum_{j=1}^{K}|h_{ij}|\right\}\\ &= \frac{\tau_k}{2}\max_i\frac{a_i}{h^\alpha}\left\{\sum_{j=1}^{i-1}\left[\frac{\alpha}{2}g_{i-j+1}+\left(1-\frac{\alpha}{2}\right)g_{i-j}\right]+\frac{\alpha}{2}g_0-\left[\frac{\alpha}{2}g_1+(1-\frac{\alpha}{2})g_0\right]\right\}\\ &\quad+\frac{\tau_k}{2}\max_i\frac{b_i}{h^\alpha}\left\{\sum_{j=i+1}^{K}\left[\frac{\alpha}{2}g_{-i+j+1}+\left(1-\frac{\alpha}{2}\right)g_{j-i}\right]+\frac{\alpha}{2}g_0-\left[\frac{\alpha}{2}g_1+(1-\frac{\alpha}{2})g_0\right]\right\}\\ &\le \eta_{\alpha,k}(a_{\max}+b_{\max})\left(\frac{\alpha^2}{2}+\frac{\alpha}{2}-1\right)\end{aligned}$$

Therefore $\left\|\frac{\tau_k}{2}H\right\|_\infty<1$ due to (3.1). This indicates that E is nonsingular. □

Our next goal is to proceed for completing the linear stability proof under constraint (3.1). For this, we need

Definition 3.1. [34,35] Let w_i^k be the exact solution of the presented finite difference method and $\tilde{w}_i^k$ be the perturbed solutions of it, where $1\le i\le K,\ 0\le k\le M,\quad K,M\in\mathbb{Z}^+$. Set $e^k=(e_1^k,e_2^k,\ldots,e_K^k)^\intercal$, where $e_i^k=w_i^k-\tilde{w}_i^k,\ 1\le i\le K$. If there is a positive integer C that for a suitable Euclidean norm $\left\|e^k\right\|\le C\left\|e^0\right\|,\ 0\le k\le M$, subject to certain constraints, then we say that the underlying method is conditionally stable under the norm.

Theorem 3.3. *Suppose* (3.1) *hold for all* $k\ge\gamma\ge 0$. *If* s *is frozen, the proposed semi-adaptive method* (2.11) *and* (2.3) *is conditionally stable.*

Proof. Denote $\xi_i^k=\tau_k a_i/(2h^\alpha),\ \lambda_i^k=\tau_k b_i/(2h^\alpha),\ i=1,2,\ldots,K,\ k=0,1,\ldots,M$. Because of (3.1) and (2.5), we observe that

$$\left(1-\frac{\alpha}{2}\right)g_0+\frac{\alpha}{2}g_1<0,\ \left(1-\frac{\alpha}{2}\right)g_{i-1}+\frac{\alpha}{2}g_i>0,\quad i=2,3,\ldots,K,$$

$$1+\xi_i^k\Big(1-\frac{\alpha}{2}\Big)g_0+\xi_i^k\frac{\alpha}{2}g_1>0,\quad i=1,2,\ldots,K,\ k=0,1,\ldots,M,$$

$$1+\lambda_i^k\Big(1-\frac{\alpha}{2}\Big)g_0+\lambda_i^k\frac{\alpha}{2}g_1>0,\quad i=1,2,\ldots,K,\ k=0,1,\ldots,M.$$

Recall Definition 3.1 and formula (2.11). if s is frozen, a straightforward computation utilizing the above leads to following identities,

$$\Big(I-\frac{\tau_k}{2}H\Big)e^{k+1}=\Big(I+\frac{\tau_k}{2}H\Big)e^k,\quad k=0,1,\ldots,M-1,$$

where H is defined in (2.7). Now we may use a mathematical induction to prove $\|e^k\|_\infty\le(1+C_1\tau_k)^k\|e^0\|_\infty$, $0\le k\le M, C_1\in\mathbb{Z}^+$. To begin, in the case of $k=1$, according to (2.5) we first obtain that

$$\begin{aligned}
\|e^1\|_\infty &= \max_{1\le j\le K}|e_j^1|=|e_\gamma^1|\le|e_\gamma^1|-\xi_\gamma^1\Big(1-\frac{\alpha}{2}\Big)\sum_{m=0}^{\gamma-1}g_m|e_\gamma^1|\ -\xi_\gamma^1\frac{\alpha}{2}\sum_{m=0}^{\gamma}g_m|e_\gamma^1|\\
&\quad-\lambda_\gamma^1\Big(1-\frac{\alpha}{2}\Big)\sum_{m=0}^{K-\gamma}g_m|e_\gamma^1|-\lambda_\gamma^1\frac{\alpha}{2}\sum_{m=0}^{K-\gamma+1}g_m|e_\gamma^1|\\
&\le\Big[1-(\xi_\gamma^1+\lambda_\gamma^1)\Big(1-\frac{\alpha}{2}\Big)g_0-(\xi_\gamma^1+\lambda_\gamma^1)\frac{\alpha}{2}g_1\Big]|e_\gamma^1|-\xi_\gamma^1\frac{\alpha}{2}g_0|e_{\gamma+1}^1|\\
&\quad-\xi_\gamma^1\sum_{m=2}^{\gamma}\Big[\Big(1-\frac{\alpha}{2}\Big)g_{m-1}+\frac{\alpha}{2}g_m\Big]|e_{\gamma-m+1}^1|\\
&\quad-\lambda_\gamma^1\frac{\alpha}{2}g_0|e_{\gamma-1}^1|-\lambda_\gamma^1\Big(1-\frac{\alpha}{2}\Big)\sum_{m=1}^{K-\gamma}g_m|e_{\gamma+m}^1|-\lambda_\gamma^1\frac{\alpha}{2}\sum_{m=2}^{K-\gamma+1}g_m|e_{\gamma+m-1}^1|\\
&\le\left[1+\xi_\gamma^0\Big(1-\frac{\alpha}{2}\Big)\sum_{m=0}^{\gamma-1}g_m+\frac{\alpha}{2}\xi_\gamma^0\sum_{m=0}^{\gamma}g_m+\lambda_\gamma^0(1-\frac{\alpha}{2})\sum_{m=0}^{K-\gamma}g_m+\lambda_\gamma^0\frac{\alpha}{2}\sum_{m=0}^{K-\gamma+1}g_m\right]\\
&\quad\times\max_{1\le j\le K}|e_j^0|\ \le\ \max_{1\le j\le K}|e_j^0|\ =\ \|e^0\|_\infty.
\end{aligned}\tag{3.2}$$

The conclusion is established naturally. In a particular case when $\|e^1\|_\infty=|e_K^1|$, utilizing (2.5) we observe that

$$\begin{aligned}
\|e^1\|_\infty &= |e_K^1|\le|e_K^1|-\xi_K^1\Big(1-\frac{\alpha}{2}\Big)\sum_{m=0}^{K-1}g_m|e_K^1|\ -\xi_K^1\frac{\alpha}{2}\sum_{m=0}^{K}g_m|e_K^1|\\
&\quad-\lambda_K^1\frac{\alpha}{2}g_0|e_K^1|-\lambda_K^1\Big[\Big(1-\frac{\alpha}{2}\Big)g_0+\frac{\alpha}{2}g_1\Big]|e_K^1|\\
&\le\Big[1-\xi_K^1\Big(1-\frac{\alpha}{2}\Big)g_0-\xi_K^1\frac{\alpha}{2}g_1\Big]|e_K^1|\\
&\quad-\xi_K^1\sum_{m=2}^{K}\Big[\Big(1-\frac{\alpha}{2}\Big)g_{m-1}+\frac{\alpha}{2}g_m\Big]|e_{K-m+1}^1|\\
&\quad-\lambda_K^1\frac{\alpha}{2}g_0|e_{K-1}^1|-\lambda_K^1\Big[\Big(1-\frac{\alpha}{2}\Big)g_0+\frac{\alpha}{2}g_1\Big]|e_K^1|\\
&\le\left\{1+\xi_K^0\Big(1-\frac{\alpha}{2}\Big)\sum_{m=0}^{K-1}g_m+\frac{\alpha}{2}\xi_K^0\sum_{m=1}^{K}g_m+\lambda_K^0\frac{\alpha}{2}g_0\right.\\
&\quad\left.+\lambda_K^0\Big[\Big(1-\frac{\alpha}{2}\Big)g_0+\frac{\alpha}{2}g_1\Big]\right\}\max_{1\le j\le K}|e_j^0|\ \le\ (1+\lambda_K^0\frac{\alpha}{2}g_0)\max_{1\le j\le K}|e_j^0|\\
&\le(1+C_1\tau_k)\ \|e^0\|_\infty.
\end{aligned}\tag{3.3}$$

Next, assume that $\|e^j\|_\infty\le(1+C_1\tau_j)^j\|e^0\|_\infty$ for $j\in\{1,2,\ldots,k-1\}$. Based on (2.5) and (3.1) for $k>1$ we must have

$$\begin{aligned}
\|e^k\|_\infty &= \max_{1\le j\le K}|e_j^k|=|e_\gamma^k|\le|e_\gamma^k|-\xi_\gamma^k\Big(1-\frac{\alpha}{2}\Big)\sum_{m=0}^{\gamma-1}g_m|e_\gamma^k|\ -\xi_\gamma^k\frac{\alpha}{2}\sum_{m=0}^{\gamma}g_m|e_\gamma^k|\\
&\quad-\lambda_\gamma^k\Big(1-\frac{\alpha}{2}\Big)\sum_{m=0}^{K-\gamma}g_m|e_\gamma^k|-\lambda_\gamma^k\frac{\alpha}{2}\sum_{m=0}^{K-\gamma+1}g_m|e_\gamma^k|
\end{aligned}$$

$$
\begin{aligned}
&\le \left[1-(\xi_\gamma^k+\lambda_\gamma^k)\Big(1-\frac{\alpha}{2}\Big)g_0-(\xi_\gamma^k+\lambda_\gamma^k)\frac{\alpha}{2}g_1\right]\big|e_\gamma^k\big|-\xi_\gamma^k\frac{\alpha}{2}g_0\big|e_{\gamma+1}^k\big| \\
&\quad-\xi_\gamma^k\sum_{m=2}^{\gamma}\left[\Big(1-\frac{\alpha}{2}\Big)g_{m-1}+\frac{\alpha}{2}g_m\right]\big|e_{\gamma-m+1}^k\big| \\
&\quad-\lambda_\gamma^k\frac{\alpha}{2}g_0\big|e_{\gamma-1}^k\big|-\lambda_\gamma^k\Big(1-\frac{\alpha}{2}\Big)\sum_{m=1}^{K-\gamma}g_m\big|e_{\gamma+m}^k\big|-\lambda_\gamma^k\frac{\alpha}{2}\sum_{m=2}^{K-\gamma+1}g_m\big|e_{\gamma-1+m}^k\big| \\
&\le \left[1+\xi_\gamma^{k-1}\Big(1-\frac{\alpha}{2}\Big)\sum_{m=0}^{\gamma-1}g_m+\frac{\alpha}{2}\xi_\gamma^{k-1}\sum_{m=0}^{\gamma}g_m+\lambda_\gamma^{k-1}\Big(1-\frac{\alpha}{2}\Big)\sum_{m=0}^{K-\gamma}g_m\right. \\
&\quad\left.+\lambda_\gamma^{k-1}\frac{\alpha}{2}\sum_{m=0}^{K-\gamma+1}g_m\right]\max_{1\le j\le K}\big|e_j^{k-1}\big| \;\le\; \max_{1\le j\le K}\big|e_j^{k-1}\big| \;=\; \big\|e^{k-1}\big\|_\infty \\
&\le (1+C_1\tau_k)\big\|e^{k-1}\big\|_\infty. \qquad (3.4)
\end{aligned}
$$

Use above inequality repeatedly. It becomes evident that

$$\big\|e^k\big\|_\infty \le (1+C_1\tau_k)^k\big\|e^0\big\|_\infty$$

for all possible $k\in\{1,2,\cdots,M\}$. In a similar way, when $\big\|e^k\big\|_\infty=\big|e_K^k\big|,\ k=0,1,\ldots,M-1$, we can secure relations

$$\big\|e^k\big\|_\infty \le (1+C_1\tau_k)\big|e_K^{k-1}\big|.$$

Therefore $\big\|e^k\big\|_\infty \le (1+C_1\tau_k)^k\big|e_K^0\big| \le e^{C_1\tau_k k}\big|e_K^0\big|$ must hold. Further, since $\tau_k k\le T$, there exists a positive integer Csuch that $\big\|e^k\big\|_\infty \le C\big\|e^k\big\|_\infty, k=0,1,\cdots,M$. Since proofs for (3.2)–(3.4) are similar, above arguments have accomplished our task. □

4. Preservations of the positivity, monotonicity

We wish to prove that the numerical solution sequence $\{w^k\}_{k=0}^M$ generated by (2.11) and (2.3) preserves required positivity and monotonicity [2,4,9,29]. To this end, we claim the following.

Lemma 4.1. *Suppose that* (3.1) *hold. If* $\tau_1<\sigma^{-1}$ *then* $w_1>w_0$ *and* $\|w_1\|_\infty<1$, *where* $\sigma=\max(s(\tau_1 s_0))$, $w_0=0$ *and* $\tau_1>0$ *is an initial temporal step.*

Proof. Please see Appendix A. □

Lemma 4.2. *Let* (3.1) *hold. If for all sufficiently small temporal step* $\tau_k>0$ *and* $0\le w_{k-1}<1$ *such that* $Hw_{k-1}+s_{k-1}>0$, *then* $\{w_k\}_{k=0}^\infty$, *the sequence of solution vectors generated by* (2.11) *and* (2.3)

(i) *forms a monotonically increasing sequence;*
(ii) *ensures that* $Hw_k+s_k>0$.

Proof. Please see Appendix B. □

Now, based on Lemmas 3.1 and 3.2, we are able to show the preservations of the solution monotonicity and positivity in following theorem.

Theorem 4.1. *Let* $k\ge\gamma\ge 0$ *and* $w_0\ge 0$. *We have*

(i) $Hw_0+s_0>0$;
(ii) *the solution sequence* $\{w_k\}_{k\ge\gamma}$ *generated by the proposed implicit scheme* (2.11) *and* (2.3) *is monotonous and increasing.*

Proof. The theorem can be obtained from Lemmas 4.1 and 4.2 directly. □

5. Simulation experiments

Two consecutive simulation examples are targeted and investigated to determine anticipated critical values in addition to the numerical solution and its temporal derivative for the two-sided space-fractional quenching problem (2.1)–(2.3). C^{++}, Fortran 90 and MATLAB programming platforms are employed. Double precision arithmetic workstations and data storages are utilized. Quenching locations, quenching times, critical domains and relationship between order of the fractional derivatives, α, of the FPDE problem are explored and analyzed.

To commence, we consider a non-degenerate case where $c_+(x,t)\equiv 0.5,\ c_-(x,t)\equiv 0.5$. For an essential assessment compared with its classical counterparts possessing integer orders, we set $\alpha=2$. The results acquired offer a straightforward, yet fundamental, examination of the accuracy and reliability of the fractional order numerical solution in a conventional manner [2,8,9,28,37].

Table 1
Selected solution values $w(a/2,t)$, $w_Z(a/2,t)$ and predicted values $\hat{w}(a/2,t)$ immediately before quenching ($a=2, \phi(x)\equiv 0$ and $T_a^*=0.78$ [3] are used).

t	$w(1.0,t)$	$w_Z(1.0,t)$	$\hat{w}(1.0,t)$	t	$w(1.0,t)$	$w_Z(1.0,t)$	$\hat{w}(1.0,t)$
0.7772	0.94041	0.94261	0.9279	0.7774	0.94261	0.94491	0.9307
0.7776	0.94491	0.94732	0.9337	0.7778	0.94732	0.94986	0.9368
0.7780	0.94986	0.95254	0.9400	0.7782	0.95254	0.95539	0.9434
0.7784	0.95539	0.95845	0.9471	0.7786	0.95845	0.96176	0.9510
0.7788	0.96176	0.96539	0.9553	0.7790	0.96539	0.96944	0.9600
0.7792	0.96944	0.97408	0.9654	0.7794	0.97408	0.97962	0.9717
0.7796	0.97962	0.98677	0.9800				

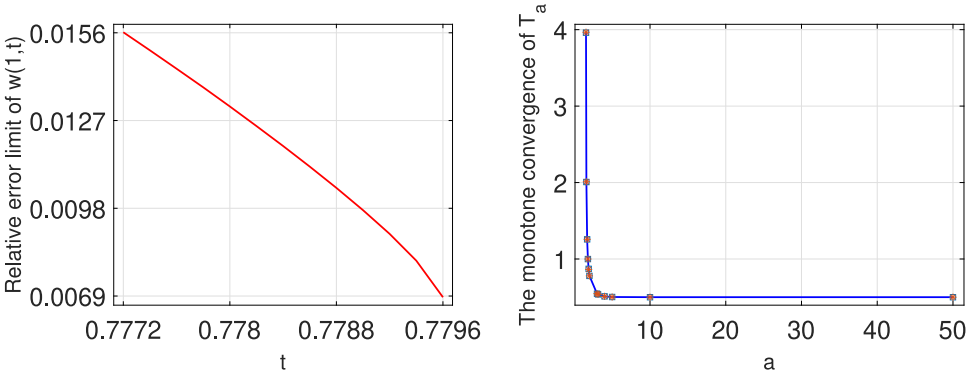

Fig. 1. LEFT: Relative difference between $w(a/2,t)$ and $w_Z(a/2,t)$ immediately before quenching; RIGHT: Trajectory of the quenching time T_a as a increases. Value points marked with ■ are recorded in [8,15]. The blue curve is for T_a values obtained in presented experiments.. (For interpretation of the references to colour in this figure legend, the reader is referred to the web version of this article.)

Table 2
Comparisons of T_a with known results $T_a^{(1)}$ [28] and $T_a^{(3)}$ [8,15]. It is observed that, as the interval size a increases, the quenching times decreases. It may be predictable that $\lim_{a\to\infty} T_a = 0.5$.

a	T_a	$T_a^{(1)}$	$T_a^{(3)}$	a	T_a	$T_a^{(1)}$	$T_a^{(3)}$
1.55	3.9660	3.9660	3.961	3.00	0.5474	0.5472	0.5460
1.60	2.0116	2.0103	2.007	π	0.5384	0.5382	0.5371
1.70	1.2574	1.2572	1.257	4.00	0.5110	0.5110	0.5110
1.80	0.9998	0.9996	0.999	5.00	0.5028	0.5026	0.5030
1.90	0.8642	0.8642	0.871	10.00	0.5006	0.5004	0.5000
2.00	0.7800	0.7798	0.779	50.00	0.5006	0.5004	0.5000

EXPERIMENT 1. Set $\alpha=2$ in (2.1)–(2.3) and (2.11), (2.3). For the purpose of comparisons, we let $\phi(x)\equiv 0$ in (2.3) [4,28].

In our experiments, the initial temporal step is chosen as $\tau_1 = 2/10^4$ and the spatial step is fixed at $h=a/10^2$. They ensure an initial CFL ratio $\lambda_1 = 1/(2a^2)$ [7,35]. The adaptation kicks in naturally as the maximum of the numerical solution exceeds a controlling parameter $\sigma = 1-\epsilon$, where $0<\epsilon\ll 1$ [29]. Our execution indicates that the critical length $a^\star \approx 1.530277$. As compared with our one-sided fractional model result $\tilde{a}^\star \approx 1.53125$ [28], the new result is apparently more closer to the standard figure, $\bar{a}^\star \approx 1.530300$, which has been used for accuracy verifications in the literature [1,6,8,11].

In the particular circumstance of $\phi(x)\equiv 0$, $a=2$, it is known that the maximal solution values $w(a/2,t)$ of (2.1)–(2.3) should follow the following estimate [3,15,28]:

$$\max_{0\le x\le a} w(x,t) = w(a/2,t) \approx \hat{w}(a/2,t) = 1-\sqrt{2(T_a^*-t)}, \quad \text{as } t\to (T_a^*)^-, \tag{5.1}$$

where T_a^* is the theoretical quenching time prediction [3]. In Table 1, we present values of the solutions $w(a/2,t)$ of the two-sided fractional Kawarada problem (2.1)–(2.3) via scheme (2.11), (2.3), $w_Z(a/2,t)$ of the one-sided fractional modeling problem [28], and the theoretical expectation $\hat{w}(a/2,t)$ shown in (5.1). It is found that the double sided numerical results are more accurate and more favorable than those via one-sided algorithm. We further plot the relative difference between two-sided and one-sided numerical solutions at $x=a/2=1$ in Fig. 1 (left frame).

As the spatial interval length a increases, the quenching time T_a decreases to approximately 0.50. More details of such monotonic decay of quenching time are given in Table 2, where T_a is for our experimentally observed quenching times; $T_a^{(1)}$ is for those obtained via one-sided fraction model [28] and $T_a^{(3)}$ is for classical results given in [8,15]. The monotone

Table 3
Additional comparisons between newly observed quenching time T_a and existing numerical results in [8,15,17,28,30] with $\alpha = 2$.

a	T_a	$T_a^{(1)}$	$T_a^{(2)}$	$T_a^{(3)}$
1.55	3.9660	3.9660	3.963	3.9610
2	0.7800	0.7798	0.779	0.7790
π	0.5384	0.5382	0.538	0.5371
10	0.5006	0.5004	0.500	0.5000

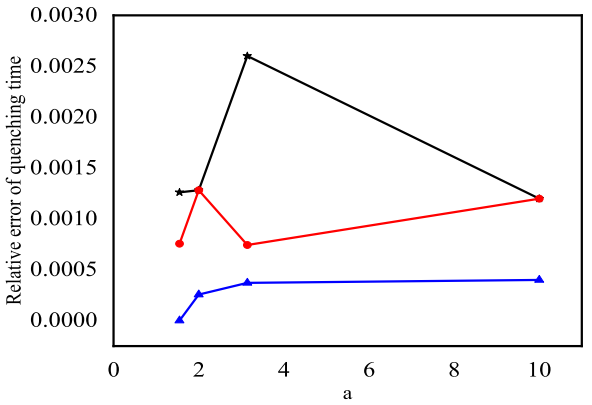

Fig. 2. Relative errors between T_a and $T_a^{(1)}$ [28], $T_a^{(2)}$ [17,30] and $T_a^{(3)}$ [8,15], respectively. Three interpolated error curves are marked with ★, • and ▲, respectively.

Table 4
Numerical values of the solution w and the derivative w_t before quenching ($\phi(x) = \sin(\pi x/2)/10,\ 0 \le x \le a$, and $a = 2$ are incorporated).

x	$w(x, T_a)$	$w_t(x, T_a)$	$w(x, T_a^{(1)})$	$w_t(x, T_a^{(1)})$
0.94	0.970127081	25.073091489	0.97012708	25.07309149
0.96	0.980947416	32.410913404	0.98094741	32.41091340
0.98	0.989067195	40.332916334	0.98906719	40.33291633
1.00	0.992266827	44.281269591	0.99226683	44.28126959
1.02	0.989067219	40.332944493	0.98906722	40.33294449
1.04	0.980947455	32.410945929	0.98094746	32.41094593
1.06	0.970127128	25.073117560	0.97012713	25.07311756

convergence of T_a from our two-sided fractional quenching model is also shown in Fig. 1 (right frame). This result coincides well with those presented in [8,15] and indicates a satisfactory consistency.

Additional comparisons are given in Table 3 for selected $a = 1.55, 2, \pi$ and 10, where $T_a^{(2)}$ values are particularly offered in [17,30]. It is evident that new values from our two-sided modeling equation are highly consistent with existing predictions. Figure 2 is devoted to the relative errors between our two-sided quenching time T_a and $T_a^{(1)}$ [28], $T_a^{(2)}$ [17,30] and $T_a^{(3)}$ [8,15], respectively. These errors are satisfactorily small hence the accuracy of T_a is clearly ensured.

Furthermore, in Fig. 3, in addition to trajectories of values of the numerical solution $\max_{0\le x\le a} w(x,t)$ and rate of change function $\max_{0\le x\le a} w_t(x,t)$ as $t \to T_a$, we also show solution cross sections in space immediately before reaching quenching ($a = 2$ and $\phi(x) = 0.1\sin(\pi x/2),\ 0 < x < a$, are used). Our semi-adaptive method (2.11), (2.3) is used and a particular $T_a \approx 0.6966$ is observed. Table 4 lists values of functions $w,\ w_t$ near the center point $x = a/2$ immediately prior to quenching. Quenching times T_a is based on our two-sided quenching model and $T_a^{(1)}$ is based on the one-sided model [28]. We may notice that the two sets of solution values are remarkably similar. Both demonstrate satisfactory geometric symmetry.

In Fig. 4, we present three-dimensional surface plots of w and w_t in last 20 temporal steps immediately before the blow-up of w_t. From Figs. 2–4, Tables 2–4 and careful comparisons with existing results we may conclude that (i) the numerical solution and associated temporal derivative function are highly accurate. They are also symmetrical in space about $x = a/2$; (ii) the terminal maximum of the numerical solution is $\max_{0\le x\le a} w(x,t) = w(a/2, T_a - \tau_k) \approx 0.992266827$ which is very close to the unity; (iii) we observe that $\sup_{0<x<a} w_t(x,t) = w_t(a/2, T_a - \tau_k) \approx 44.281269591$ as $t \to T_a$. The computation is throughout smooth. The phenomenon is typical in quenching simulations. These coincide precisely with existing theoretical and computational predictions given in numerous recent publications, for instance, in [6,8,15,28,30]. Therefore our two-sided model and algorithm (2.11), (2.3) are effective and reliable.

Experiment 2.

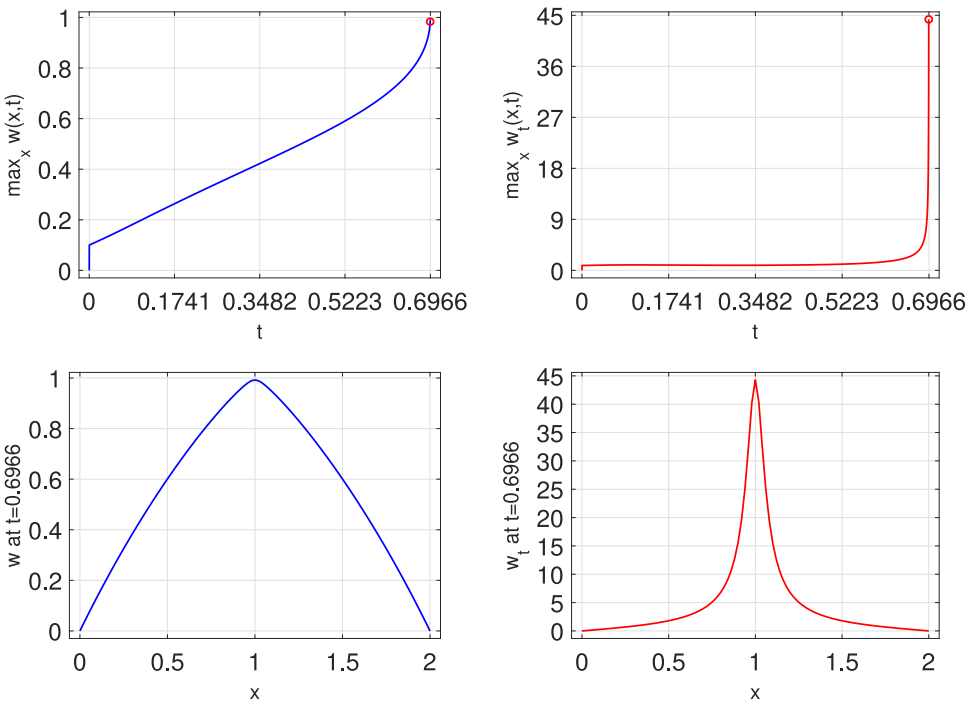

Fig. 3. TOP: trajectories of $\max_{0\le x\le a} w$ and $\sup_{0<x<a} w_t$ as the time t increasing to T_a. BOTTOM: Functions w and w_t at $t = T_a - \tau_k$ immediately before quenching. (w is colored blue and w_t is colored red. Parameters $a = 2,\ \alpha = 2,\ T_a \approx 0.6966$ are used/observed). (For interpretation of the references to colour in this figure legend, the reader is referred to the web version of this article.)

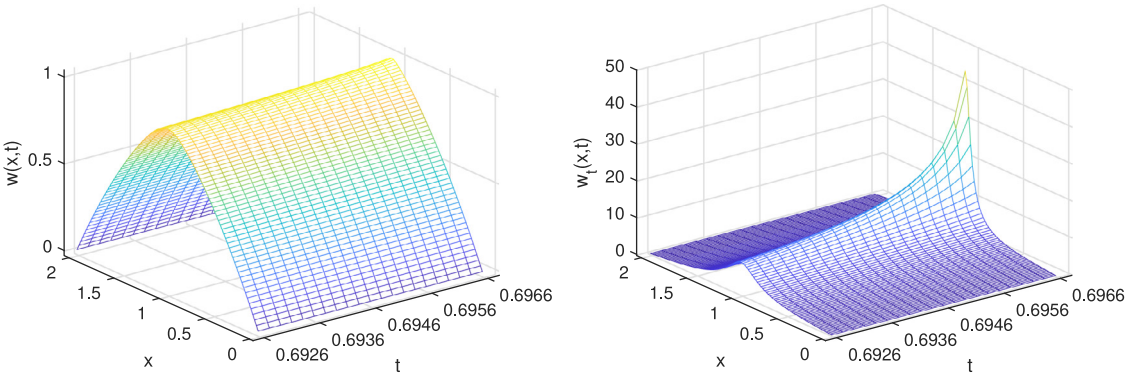

Fig. 4. Three-dimensional surface plots of the quenching solutions w and derivative w_t on the final 20 solution vectors prior to quenching. The terminal supremum of w_t is approximately 44.281269591. A typical quenching case is evident ($0 \le x \le a,\ 0.6926 \le t \le 0.6966,\ a = 2$).

In this experiment, we consider multiple values of $\alpha \in \left[(\sqrt{17}-1)/2, 2\right)$ for the two-sided space-fractional order diffusion problem (2.1)–(2.3). We note that this represents a fast diffusive physical procedure, where particles may move more rapidly than those in classical cases of Experiment 1 [32]. The new solution to obtain can be highly vibrated in multi-physics and hydrology [20,22,31]. Again, we adopt the semi-adaptive simulation method (2.11), (2.3).

Take $a = 2$. We begin with an initial function $\phi(x) = 0.1\sin(\pi x/2),\ 0 \le x \le a$, with the fractional order $\alpha = 1.7, 1.8, 1.9$, respectively. In Fig. 5, we again demonstrate trajectories of $\max_{0\le x\le a} w$ and $\sup_{0<x<a} w_t$ as time t approaches the numerical quenching time found, that is, T_a. Order $\alpha = 1.8$ is used. Furthermore, we can notice that, while $\max_{0\le x\le a} w$ approaches the unity smoothly, the supremum of w_t climbs to a peak, probably faster than exponentially [6], at heights approximately $44.7816,\ 51.6743,\ 38.5741$, respectively in cases of $\alpha = 1.7, 1.8, 1.9$. To view more details, we plot profiles of the numerical solution w and its rate of change function w_t, corresponding to cases of various α values in Fig. 6. We observe again that quenching all locations are precisely at the center of spatial interval, that is, at $x_a = 1$, probably due to lacking of non-symmetric degeneracy [29,30]. We remark that peak values $w(a/2, t)$ immediately before quenching are pretty close to the unity. For example, for the cases when $\alpha = 1.7, 1.8, 1.9$, we have $w(a/2, T_a - \tau_k) \approx 0.9897628,\ 0.994449,\ 0.987745$, respectively.

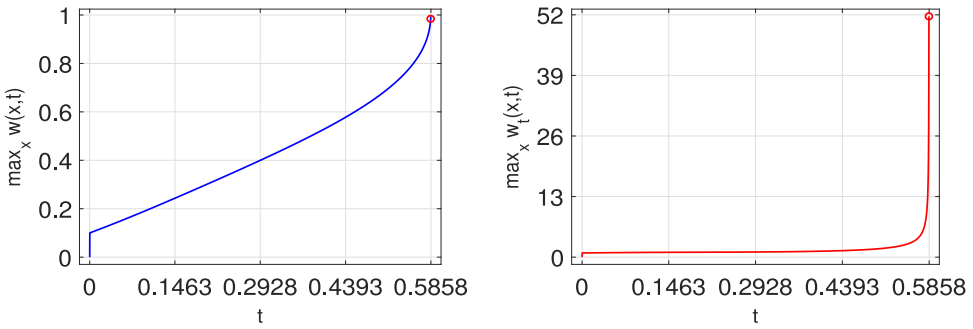

Fig. 5. Trajectories of $\max_{0\le x\le a} w$ (LEFT) and $\sup_{0<x<a} w_t$ as $t \to T_a$ (RIGHT). Parameters used: $\alpha = 1.8$, $T_a \approx 0.5858$ and $a = 2$.

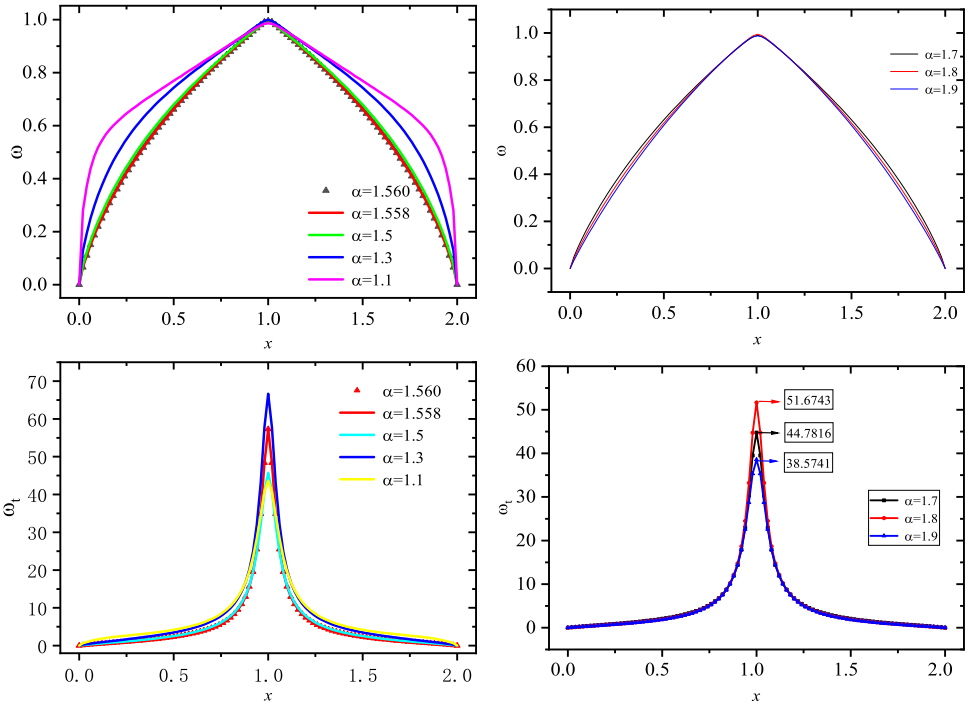

Fig. 6. TOP: solutions $w(x, T_a - \tau_k)$ immediately before quenching (LEFT for $\alpha = 1.1, 1.3, 1.5, 1.558, 1.560$; RIGHT for $\alpha = 1.7, 1.8, 1.9$); Bottom: derivative functions $w_t(x, T_a - \tau_k)$ (LEFT for $\alpha = 1.1, 1.3, 1.5, 1.558, 1.560$; RIGHT for $\alpha = 1.7, 1.8, 1.9$). Although geometric patterns of w seem to be different between cases of $\alpha < (\sqrt{17}-1)/2 \approx 1.561552$ and $\alpha > (\sqrt{17}-1)/2 \approx 1.561552$, the excellent symmetry can always be observed.

To further illustrate interesting characteristics of a quenching solution, in Fig. 7 we present three-dimensional surface plots based on the final 20 time steps prior to quenching. It is evident that both w and w_t are not only monotonically increasing but also symmetric with respect to the space center at $x = a/2$.

Throughout Experiment 2, we notice that anticipated quenching phenomena do occur for the various fractional derivative orders $\alpha \in (1, 2]$ used, as far as the interval size $a \ge a^*$ which is a critical value depending on the particular value of α. The positivity, monotonicity and symmetry of the numerical solution w and its temporal derivative w_t are well preserved whenever the initial value is symmetric. In the circumstance, locations of $\max_{0\le x\le a} w(x,t)$, $\sup_{0<x<a} w_t(x,t)$ appear to be at the geometric center of the spacial interval. The semi-adaptive simulation procedure (2.11), (2.3) remain to be numerically stable for solving the two-sided nonlinear fractional quenching model problem (2.1)–(2.3).

Let T_a and $\hat{T}_a$ be quenching times derived via our two-sided and one-sided fractional models and corresponding numerical methods, respectively [28]. As an illustration, in Table 5, we list and compare quenching times with different spatial interval lengths and $\alpha \in [1.6, 2]$. It is not difficult to see that T_a decreases monotonically just like $\hat{T}_a$ does as α decreases. The magnitudes of T_a seem to be slightly less than its peers', though we may not be able to conclude a common limit 0.5 as in Experiment 1. Figure 8 illustrates connections of quenching times, critical domain sizes and the fractional order $\alpha \in [1.6, 2]$, respectively. The phenomena observed are highly in agreement with existing simulations [5,28,29].

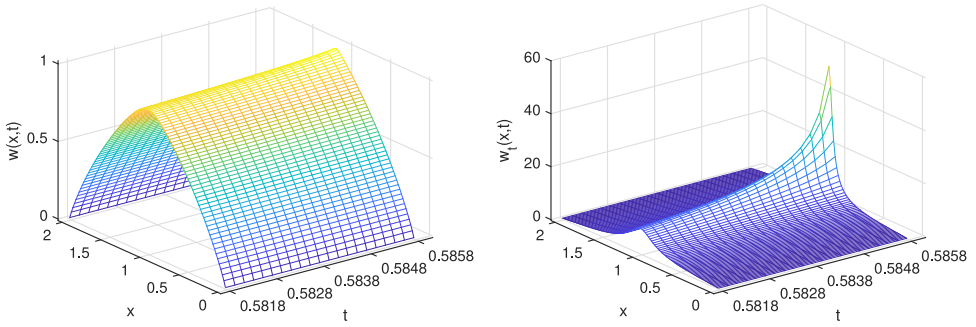

Fig. 7. 3D surface plots of the quenching solutions w and associated derivative w_t on the final 20 solution vectors prior to a blow-up of w_t. ($0 \le x \le a,\ 0.5818 \le t \le 0.5858,\ a = 2$). The height of w_t peak is approximately 51.674333376. A typical quenching phenomenon is thus observed.

Table 5
Comparisons between $T_a, \hat{T}_a$ and their connections with the fractional order α. Spatial interval sizes $a = 1.55, 2, \pi$ and 10 are utilized.

α	2.0	1.95	1.90	1.85	1.80
$T_{1.55}/\hat{T}_{1.55}$	3.8724/3.966	1.9228/2.0544	1.3830/1.5364	1.1080/1.2716	0.9370/1.104
$T_2/\hat{T}_2$	0.6966/ 0.7798	0.6658/0.7494	0.6368/0.7224	0.6102/0.6978	0.5858/0.6752
$T_\pi/\hat{T}_\pi$	0.5016/0.5382	0.4998/0.5368	0.4974/0.5352	0.4948/0.5334	0.4916/0.5316
$T_{10}/\hat{T}_{10}$	0.4682/0.5004	0.4672/ 0.5006	0.4662/0.5008	0.4668/0.5008	0.4632/0.501
α	1.75	1.70	1.65	1.60	
$T_{1.55}/\hat{T}_{1.55}$	0.8194/0.9856	0.7332/0.8956	0.6676/0.8236	0.6164/0.7644 -	
$T_2/\hat{T}_2$	0.5636/0.6546	0.5436/0.6354	0.5258/0.6174	0.5100/0.6008 -	
$T_\pi/\hat{T}_\pi$	0.4882/0.5294	0.4842/0.5274	0.4798/0.5252	0.5100/0.5230 -	
$T_{10}/\hat{T}_{10}$	0.4614/0.5012	0.4594/ 0.5012	0.4570/ 0.5014	0.4542/ 0.5014 -	

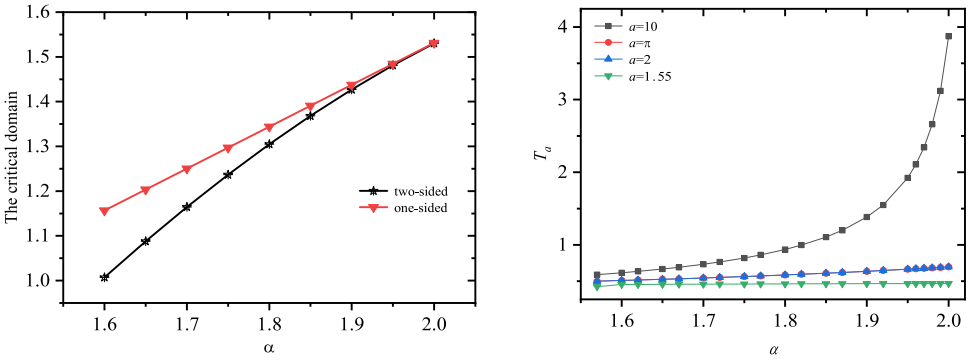

Fig. 8. LEFT: Critical sizes corresponding to the two-sided and one-sided model problems vs. the fractional order α; RIGHT: Quenching times T_a corresponding to the two-sided model problem vs. the fractional order α.

Table 6
Computed relations between quenching times T_a and fractional order α.

α	1.57	1.568	1.566	1.564	1.562	1.560	1.558	1.50	1.30	1.10
$T_{1.55}$	0.5910	0.5894	0.5878	0.5862	0.5846	0.5832	0.5816	0.5432	0.4636	0.4214
T_2	0.5014	0.5010	0.5004	0.4998	0.4992	0.4988	0.4982	0.4838	0.4466	0.4180
T_π	0.4720	0.4718	0.4716	0.4714	0.4712	0.4710	0.4708	0.4646	0.4410	0.4170
T_{10}	0.4526	0.4524	0.4522	0.4522	0.4520	0.4520	0.4518	0.4480	0.4326	0.4148

It is known that quenching solutions of classical problems are symmetric with respect to $x = a/2$ if initial and boundary data used are symmetric [1,4,6,10]. Preservations of such geometric feature have been extremely challenging issues in simulations. Our intensive simulation experiments indicate that our two-sided model and method are more capable of such preservation as compared with one-sided model and method. To see this, we show quenching locations $x_\alpha,\ (\sqrt{17}-1)/2 \le \alpha < 2$, with respect to different interval lengths a in Table 7. As a comparison, we also list computed quenching locations $\hat{x}_{1.6}, \hat{x}_{1.8}$ obtained via the one-sided model and method [28]. Data are taken immediately before quenching.

Table 7
Quenching locations associated with different domain sizes and different fractional orders. Locations x_α, $\alpha \in \left[(\sqrt{17}-1)/2, 2\right)$, are from new two-sided model and method, while $\hat{x}_{1.6}, \hat{x}_{1.8}$ are due to one-sided model and method [28].

$x_\alpha \backslash a$	1.55	2	π	4	5	8	10	50
x_α	0.775	1.00	1.57079625	2.00	2.50	4.00	5.00	25.00
$\hat{x}_{1.8}$	0.63549998	0.84	1.50796795	2.04	2.75	5.2	7.0	45
$\hat{x}_{1.6}$	0.51149998	0.76	1.53938395	2.2	3.0	6.68	7.5	45.5

Table 8
A correlation of critical values $a^\star$ (due to to the two-sided model and method), $a_Z^\star$ (due to one-sided model and method) and the fractional order α. Here $\Delta a^\star$ and $\Delta a_Z^\star$ are differences between two consecutive critical values calculated via respective methods, respectively.

α	2	1.95	1.90	1.85	1.80	1.75	1.70	1.65	1.60
$a^\star$	1.53027	1.481027	1.426962	1.368171	1.30471	1.236725	1.164345	1.087762	1.007221
$\Delta a^\star$	–	0.049243	0.054065	0.058791	0.06346	0.067985	0.072380	0.076583	0.080541
$a_Z^\star$	1.53125	1.48437	1.43755	1.39076	1.34398	1.29718	1.25038	1.20355	1.15666
$\Delta a_Z^\star$	–	0.04688	0.04682	0.04679	0.04678	0.04680	0.04680	0.04683	0.04689

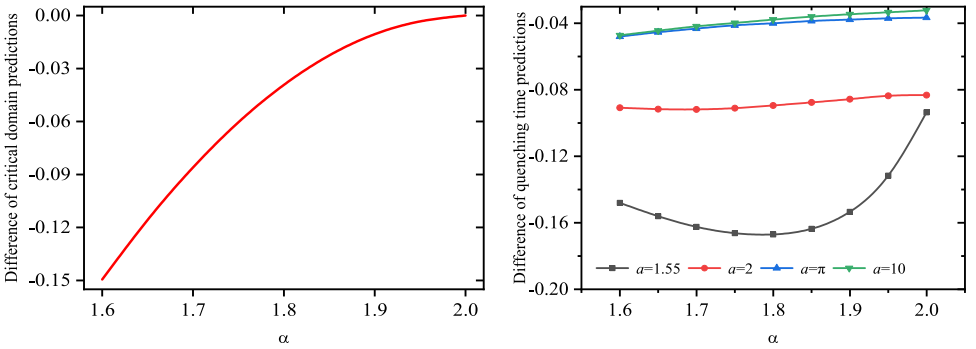

Fig. 9. LEFT: Difference between predicted critical domains via one-sided and two-sided models and methods; RIGHT: Difference between predicted quenching times via one-sided and two-sided models and methods.

There is no surprise to see that while x_α, $(\sqrt{17}-1)/2 \le \alpha < 2$, offers clearly an anticipated symmetry with respect to underlying spatial geometric centers, $\hat{x}_{1.6}, \hat{x}_{1.8}$ depart away from the preservation, though the error margins are small. The superiority of x_α indicates not only a better preservative feature, but also a more balanced approximation of the physical phenomena [11,33]. To conclude, simulations based on the two-sided model and method can be more accurate and reliable as compared with existing one-sided fractional formulations.

Let $a^\star, a_Z^\star$ be computed critical domain sizes via the two-sided fractional model and numerical method, and one-sided fractional model and corresponding numerical method [2,28], respectively. Table 8 is tailored for showing probable interconnections between the fractional order α and aforementioned sizes. We find that the critical interval sizes decrease as α decreases. It is observed that differences between consecutive values calculated are between 0.049243 and 0.080541 as the value of α increases from $(\sqrt{17}-1)/2$ to 2. The limit of $a^\star$ is well-anticipated [28]. We may conclude numerically that smaller critical domain sizes should be expected for lower fractional orders in both two-sided and one-sided cases. Furthermore, critical domain sizes corresponding to two-sided models are less than that in their one-sided counterparts. In Fig. 9, differences in predicted critical domain between the two-sided and one-sided strategies are shown on the left, while differences between predicted quenching times are shown on the right. The results are in good agreement with existing theory and computations [6–8,15,28–30].

Now, recall Fig. 6 and Table 6. Computational results and quenching times for different interval size a are given even for cases where order $\alpha < (\sqrt{17}-1)/2 \approx 1.561552$. Although our simulations utilizing (2.11), (2.3) are accurate, stable and highly successful for $\alpha \in \left(1, (\sqrt{17}-1)/2\right)$, corresponding theoretical proofs are extremely difficult to fulfill due to limitations of the maximal principal used [23,24]. This no doubt remains as a continuing challenge to our endeavors.

6. Conclusions

An efficient numerical method for a quenching type diffusion equation associated with a two-sided Riemann-Liouville spatially fractional derivative is studied. Discretization of the two-sided fractional derivative is implemented via weighted and averaged standard and shifted Grünwald formulas. Resulted semi-discretized system of ordinary equations is then approximated via a trapezoidal rule and at the same time, matrix exponential operators involved are handled through proper

Padé approximants. These result a second-order Crank-Nicolson type method, equipped with a temporal arc-length adaptation strategy ensuring additional accuracy and reliability for precisely capturing the singular solution of the fractional Kawarada modeling Eq. (2.1).

Preservations of the discrete solution stability, monotonicity and positivity are analyzed, proved, and validated through sequences of simulation experiments. Stability conditions of the temporally adaptive finite difference method are established for $\alpha \in \left((\sqrt{17}-1)/2, 2\right]$ targetting super-diffusive applications where particles diffuse faster than usual cases.

Two interconnected sets of simulation experiments are designed and conducted. They demonstrate remarkably the capability and accuracy of the two-sided fractional differential equation based method constructed. The integer order $\alpha = 2$ is considered in our first experiment. In the circumstance, numerical solution and data generated can be directly compared to the best known solutions of integer order problems for accuracy and credibility. It is noticed that the critical size $a^\star \approx 1.530277$ and corresponding quenching time $T_{a^\star} \approx 0.7800$ in our study are precisely in agreement with known results in the literature [1,6,11,15,28]. Our second round of experiments is then progressed to cases with non-integer orders $\alpha \in \left[(\sqrt{17}-1)/2, 2\right)$. In the situations, numerical solutions obtained are compared with those from similar, but less mature, one-sided fractional quenching model and methods. Our computations are focused on vital characteristics of the quenching solutions of the singular modeling differential equation equipped with two-sided fractional derivative. Properties of the numerical solution, its analysis and connections with the fractional order α are investigated. In addition, we find that the two-sided fractional derivative based model and simulation method are superior as compared with their one-sided counterparts. We also find that the size of critical intervals decreases monotonically as the order α decreases. Both sets of experiments show that the two-sided space-fractional model and method may provide more balanced and accurate approximations of quenching phenomena as compared with conventional fractional strategies.

Based on optimistic simulation results, we intend to extend our rigorous analysis to cases where $\alpha \in \left(1, (\sqrt{17}-1)/2\right]$ in our forthcoming paper. Further explorations will be extended to multidimensional and multiple-sided space-fractional modeling equations. Though such considerations can be extremely meaningful especially in realistic applications, the challenges involved can be enormous. First of them can be in theoretical analysis and dynamic property studies. Then, due to the non-local features of fractional-order derivatives, large and dense matrices may be resulted from discretization, even under hybrid settings [33]. This may require more sensitive quenching algorithmic strategies, such as the fast multipole and Krylov subspace implementations, and operator splitting techniques into our research agendas. Free energy conservation analysis may also be approached for potential biomedical and microbiology applications [18,27,32].

Acknowledgments

The first and the second authors are supported in part by NSFC Research Grant (No. 12062024, China) and NSFC of Ningxia Province Research Grant (No. 2020AAC03069, China). The third author is supported in part through an URC Research Award (No. 2021-CAS03) from Baylor University (USA). The authors would express their sincere thanks to the anonymous referees for extremely valuable comments and suggestions that improve the quality and presentation of this paper.

Appendix A. Proof of Lemma 4.1

Proof. Based on (2.11), we have

$$w_k = \left(I - \frac{\tau_k}{2}H\right)^{-1}\left(I + \frac{\tau_k}{2}H\right)\left(w_{k-1} + \frac{\tau_k}{2}s_{k-1}\right) + \frac{\tau_k}{2}s_k.$$

Firstly, recall Theorems 3.1 and 3.2. We must have

$$\begin{aligned} w_1 &= \left(I - \frac{\tau_1}{2}H\right)^{-1}\left(I + \frac{\tau_1}{2}H\right)\left(w_0 + \frac{\tau_1}{2}s_0\right) + \frac{\tau_1}{2}s_1 \\ &= \frac{\tau_1}{2}\left[\left(I - \frac{\tau_1}{2}H\right)^{-1}\left(I + \frac{\tau_1}{2}H\right)s_0 + s(\tau_1 s_0)\right] \;>\; w_0 \;=\; 0. \end{aligned}$$

Define $Y = (1, 1, \ldots, 1)^\intercal \in \mathbb{R}^K$ and consider the difference between w_1 and Y. To show $\|w_1\|_\infty < 1$ we consider

$$\begin{aligned} w_1 - Y &= \frac{\tau_1}{2}\left[\left(I - \frac{\tau_1}{2}H\right)^{-1}\left(I + \frac{\tau_1}{2}H\right)s_0 + s(\tau_1 s_0)\right] - Y \\ &= \left(I - \frac{\tau_1}{2}H\right)^{-1}\left[\frac{\tau_1}{2}\left(I + \frac{\tau_1}{2}H\right)s_0 + \frac{\tau_1}{2}\left(I - \frac{\tau_1}{2}H\right)s(\tau_1 s_0)\right. \\ &\quad \left. - (I - \frac{\tau_1}{2}H)Y\right]. \end{aligned}$$

Secondly, we denote

$$Z_1 = \frac{\tau_1}{2}\left(I + \frac{\tau_1}{2}H\right)s_0 + \frac{\tau_1}{2}\left(I - \frac{\tau_1}{2}H\right)s(\tau_1 s_0),$$

$$Z_2 = -\Big(I - \frac{\tau_1}{2}H\Big)Y,$$
$$Z_0 = Z_1 + Z_2.$$

It follows immediately that

$$\begin{aligned} Z_1 &= \frac{\tau_1}{2}\Big(I + \frac{\tau_1}{2}H\Big)s_0 + \frac{\tau_1}{2}\Big(I - \frac{\tau_1}{2}H\Big)s(\tau_1 s_0) \\ &\le \frac{\tau_1}{2}\Big[\Big(I + \frac{\tau_1}{2}H\Big) + \Big(I - \frac{\tau_1}{2}H\Big)\Big]s(\tau_1 s_0) \;=\; \tau_1 s(\tau_1 s_0). \end{aligned} \tag{A.1}$$

Recall (2.5) and the fact that $\sum_{j=0}^{i} g_j \le \sum_{j=0}^{\infty} g_j = 0$. We acquire that $HY \le 0$. Hence,

$$Z_2 = -Y + \frac{\tau_1}{2}HY \le -Y.$$

Thirdly, based on the above result and (A.1), we observe that $Z_0 \le \tau_1 s(\tau_1 s_0) - Y < \tau_1 \max(s(\tau_1 s_0)) - 1 = \tau_1\sigma - 1$. Now, for $\tau_1 < \sigma^{-1}$, we obtain that $Z_0 < 0$. It follows subsequently that $w_1 - Y = \big(I - \frac{\tau_1}{2}H\big)^{-1}Z_0$. Recall that the matrix $I - \frac{\tau_1}{2}H$ is inverse positive due to Theorem 3.1. Thus $\|w_1\|_\infty < 1$ is true. This completes our proof. □

Appendix B. Proof of Lemma 4.2

Proof. Note that $w_1 > w_0$ due to Lemma 4.1. Next, by an Euler formula, we may approximate s_k in (2.11) through $s_k = s_{k-1} + \tau_k C_2(Hw_{k-1} + s_{k-1}) + \mathcal{O}(\tau_k^2),\ k \ge 1$. Furthermore, according to (2.11), we must have

$$\begin{aligned} w_k - w_{k-1} &= \Big(I - \frac{\tau_k}{2}H\Big)^{-1}\Big[\Big(I + \frac{\tau_k}{2}H\Big)\Big(w_{k-1} + \frac{\tau_k}{2}s_{k-1}\Big) \\ &\quad + \frac{\tau_k}{2}\Big(I - \frac{\tau_k}{2}H\Big)s_k - \Big(I - \frac{\tau_k}{2}H\Big)w_{k-1}\Big] \\ &\ge \tau_k\Big(I - \frac{\tau_k}{2}H\Big)^{-1}\Big[Hw_{k-1} + s_{k-1} - \frac{\tau_k}{4}H(s_k - s_{k-1})\Big],\ \ k > 1. \end{aligned} \tag{B.1}$$

Since $s_k > s_{k-1}$, by means of Taylor's theorem [16], we acquire following inequality for $k > 1$,

$$w_k - w_{k-1} \ge \tau_k\Big(I - \frac{\tau_k}{2}H\Big)^{-1}\Big[(Hw_{k-1} + s_{k-1}) - \frac{C_2\tau_k^2}{4}H(Hw_{k-1} + s_{k-1})\Big],$$

where C_2 is the positive diagonal Jacobian matrix of $s(w)$ after at some mean value point was evaluated. Subsequently $w_k > w_{k-1}$ if $\tau_k > 0$ is sufficiently small. Likewise, it is readily to see that

$$\begin{aligned} Hw_k + s_k &= Hw_k + Hw_{k-1} - Hw_{k-1} + s_k + s_{k-1} - s_{k-1} \\ &= s_k - s_{k-1} + Hw_{k-1} + s_{k-1} \\ &\quad + H\Big[\Big(I - \frac{\tau_k}{2}H\Big)^{-1}\Big(I + \frac{\tau_k}{2}H\Big)\Big(w_{k-1} + \frac{\tau_k}{2}s_{k-1}\Big) + \frac{\tau_k}{2}s_k - w_{k-1}\Big] \\ &= s_k - s_{k-1} + \Big(I - \frac{\tau_k}{2}H\Big)^{-1}\Big[\Big(I - \frac{\tau_k}{2}H\Big)(Hw_{k-1} + s_{k-1}) \\ &\quad + \tau_k H^2 w_{k-1} + \frac{\tau_k}{2}H(s_{k-1} + s_k) + \frac{\tau_k^2}{4}H^2(s_{k-1} - s_k)\Big] \\ &\ge s_k - s_{k-1} + \Big(I - \frac{\tau_k}{2}H\Big)^{-1}\Big[\Big(I + \frac{\tau_k}{2}H\Big)(Hw_{k-1} + s_{k-1}) \\ &\quad + \frac{\tau_k^2}{4}H^2(s_{k-1} - s_k)\Big]. \end{aligned} \tag{B.2}$$

Since $s_k \approx s(w_{k-1} + \tau_k(Hw_{k-1} + s_{k-1}))$ and $s_k > s_{k-1}$, again by Taylor's theorem, we find that

$$\begin{aligned} Hw_k + s_k &\ge s_k - s_{k-1} + \Big(I - \frac{\tau_k}{2}H\Big)^{-1}\Big(I - \frac{\tau_k}{2}H\Big)\Big(I + \tau_k H - \frac{C_2\tau_k^3}{4}H^2\Big) \\ &\quad \times (Hw_{k-1} + s_{k-1}) \\ &= s_k - s_{k-1} + \Big(I + \tau_k H - \frac{C_2\tau_k^3}{4}H^2\Big)(Hw_{k-1} + s_{k-1}). \end{aligned}$$

Therefore the matrix $I + \tau_k H - \frac{\tau_k^3}{4}C_2H^2$ must be positive for sufficiently small $\tau_k > 0$. Our lemma is thus clear. □

.

References

[1] A. Acker, W. Walter, The quenching problem for nonlinear parabolic differential equations, Lect. Notes Math. 564 (1976) 1–12.
[2] H. Cheng, P. Lin, Q. Sheng, R. Tan, Solving degenerate reaction-diffusion equations via variable step Peaceman-Rachford splitting, SIAM J. Sci. Comput. 25 (2003) 1273–1292.
[3] S. Filippas, J.S. Guo, Quenching profiles for one-dimensional semilinear heat equations, Quart. Appl. Math. 51 (1992) 94–103.
[4] J.K. Hale, Asymptotic Behavior of Dissipative Systems, American Math Soc., 1988.
[5] J.L. Padgett, Solving degenerate stochastic kawarada partial differential equations via adaptive splitting methods, 2017.
[6] H. Kawarada, On solutions of initial-boundary value problems for $u_t = u_{xx} + \frac{1}{1-u}$, Publ Res. Inst. Math. Sci. 10 (1975) 729–736.
[7] J.L. Padgett, The quenching of solutions to time-space fractional Kawarada problems, Comput. Math. Appl. 76 (2018) 1583–1592.
[8] Q. Sheng, Adaptive decomposition finite difference methods for solving singular problems, Front. Math. China 4 (2009) 599–626.
[9] Y. Xu, Quenching phenomenon in a fractional diffusion equation and its numerical simulation, Intern J. Comput. Math. 95 (2018) 98–113.
[10] C.Y. Chan, C.S. Chen, A numerical method for semi-linear singular parabolic mixed boundary value problems, Quart. Appl. Math. 47 (1989) 45–57.
[11] Q. Sheng, A. Khaliq, Linearly implicit adaptive schemes for singular reaction-diffusion equations, in: A.V. Wouwer, Ph. Saucez, W.E. Schiesser (Eds.), Adaptive Methods of Lines, CRC Press, London and New York, 2001, pp. 274–305.
[12] W. Walter, Parabolic differential equations with a singular nonlinear term, Funkcial Ekvac. 19 (1976) 271–277.
[13] W. Huang, Y. Ren, R.D. Russell, Moving mesh partial differential equations (MM-PDEs) based on the equidistribution principle, SIAM J. Numer. Anal. 31 (1994) 709–730.
[14] J.L. Padgett, Q. Sheng, Nonuniform Crank-Nicolson scheme for solving the stochastic Kawarada equation via arbitrary grids, Numer. Meth. PDEs 33 (2017) 1305–1328.
[15] Q. Sheng, A. Khaliq, A compound adaptive approach to degenerate nonlinear quenching problems, Numer. Meth. PDEs 35 (1999) 29–47.
[16] A. Khaliq, E.H. Twizell, D.A. Voss, On parallel algorithms for semidiscretized parabolic partial differential equations based on subdiagonal Padé approximations, Numer. Meth. PDEs 9 (1993) 107–116.
[17] J.W. Mooney, A numerical method for accurate critical length estimation in singular quenching problems, Dyn. Sys. Appl. 4 (1995) 505–516.
[18] N. Garcia-Montoya, J. Kabre, J.E. Macías-Díaz, Q. Sheng, Second-order semi-discretized schemes for solving stochastic quenching models on arbitrary spatial grids, Discrete Dyn. Nature Soc. 21 (2021) 553–571.
[19] J. Zhou, Quenching for a parabolic equation with variable coefficient modeling MEMS technology, Appl. Math. Comput. 314 (2017) 7–11.
[20] I. Podlubny, Fractional Differential Equations, first ed., Academic Press, San Diego, CA, 1998.
[21] R. Martínez, J.E. Macías-Díaz, Q. Sheng, A nonlinear discrete model for approximating a conservative multi-fractional Zakharov system: analysis and computational simulations, Math. Comput. Simul. 202 (2022) 1–21.
[22] M.M. Meerschaert, C. Tadjeran, Finite difference approximations for two-sided space-fractional partial differential equations, Appl. Numer. Math. 56 (1) (2006) 80–90.
[23] L. Zhu, H. Rui, A kind of second-order implicit finite difference methods for two-sided space fractional partial differential equations based on maximum modulus principle, J. Chongqing Normal Univ. (Natural Science) 32 (2015) 466–478.
[24] L. Zhu, H. Rui, Maximum modulus principle estimates for one dimensional fractional diffusion equation, Appl. Math. J. Chinese Univ. 30 (2015) 99–106.
[25] M.M. Meerschaert, C. Tadjeran, Finite difference approximations for fractional advection-dispersion flow equation, J. Comput. Appl. Math. 172 (2004) 65–77.
[26] J.E. Macías-Díaz, R. Martínez, Q. Sheng, An implicit semi-linear discretization of a bi-fractional Klein-Gordon-Zakharov system which conserves the total energy, Appl. Numer. Math. 169 (2021) 179–200.
[27] H. Hejazi, T. Moroney, F.W. Liu, A finite volume method for solving the two-sided time-space fractional advection-dispersion equation, Centr. Eur. J. Phys. 11 (2013) 1275–1283.
[28] L. Zhu, Q. Sheng, A note on the adaptive numerical solution of a Riemann-Liouville space-fractional Kawarada problem, J. Comput. Appl. Math. 374 (2020) 466–478.
[29] M.A. Beauregard, Numerical approximations to a fractional Kawarada quenching problem, Appl. Math. Comput. 348 (2019) 14–22.
[30] Q. Sheng, Y. Ge, A numerical endeavor with nonlinear Kawarada equations, Dyn. Sys. Appl. 25 (2016) 543–556.
[31] B.L. Guo, X.K. Pu, F. Huang, Fractional Partial Differential Equations and Their Numerical Solutions, World Scientific, Singapore, 2015.
[32] A. Chaves, Fractional diffusion equation to describe Lévy flights, Phys. Lett. A 239 (1998) 13–16.
[33] Q. Sheng, Hybrid approximations via second order combined dynamic derivatives on time scales, Electro. J. Qual. Theor. Diff. 17 (2007) 1–13.
[34] A. Iserles, A First Course in the Numerical Analysis of Differential Equations, second ed., Cambridge University Press, Cambridge and London, 2009.
[35] R. LeVeque, Finite Difference Methods for Ordinary and Partial Differential Equations: Steady-State and Time-Dependent Problems, SIAM, Philadelphia, PA, 2007.
[36] M.A. Beauregard, Q. Sheng, An adaptive splitting approach for the quenching solution of reaction-diffusion equations over nonuniform grids, J. Comput. Appl. Math. 241 (2013) 30–44.
[37] Y. Xu, H. Sun, Q. Sheng, On variational properties of balanced central fractional derivatives, Intern J. Comput. Math. 95 (2018) 39–67.